Femtosecond-pulsed optical heating of gold nanoparticles

Guillaume Baffou* and Hervé Rigneault

Institut Fresnel, CNRS, Aix-Marseille Université, École Centrale de Marseille, Domaine Universitaire Saint-Jérôme, F-13397 Marseille, France

(Received 10 March 2011; revised manuscript received 29 April 2011; published 21 July 2011)

We investigate theoretically and numerically the thermodynamics of gold nanoparticles immersed in water and illuminated by a femtosecond-pulsed laser at their plasmonic resonance. The spatiotemporal evolution of the temperature profile inside and outside is computed using a numerical framework based on a Runge-Kutta algorithm of the fourth order. The aim is to provide a comprehensive description of the physics of heat release of plasmonic nanoparticles under pulsed illumination, along with a simple and powerful numerical algorithm. In particular, we investigate the amplitude of the initial instantaneous temperature increase, the physical differences between pulsed and cw illuminations, the time scales governing the heat release into the surroundings, the spatial extension of the temperature distribution in the surrounding medium, the influence of a finite thermal conductivity of the gold/water interface, the influence of the pulse repetition rate of the laser, the validity of the uniform temperature approximation in the metal nanoparticle, and the optimum nanoparticle size (∼40 nm) to achieve a maximum temperature increase.

DOI: 10.1103/PhysRevB.84.035415 PACS number(s): 65.80.−g, 73.20.Mf, 44.05.+e

I. INTRODUCTION

Gold nanoparticles (NPs) can act as efficient nanosources of heat under visible or infrared illumination at the plasmonic resonance due to enhanced light absorption.[1] The ability to locally heat at the nanoscale opens the path for promising achievements in nanotechnology and especially for nanoscale control of temperature distribution,[2] chemical reactions,[3] phase transition,[4] material growth,[5] photothermal cancer therapy,[6–8] and drug release.[9,10]

The use of femtosecond-pulsed illumination on gold NPs expands the range of applications compared to continuous (cw) illumination. First, it can lead to nonlinear optical processes such as two-photon luminescence or second harmonic generation with applications mainly in bioimaging.[11,12] Then, it can trigger a sudden temperature increase at the subnanosecond scale and subsequent effects such as acoustic waves used for optoacoustic imaging[13,14] or bubble formation for nanosurgery.[15] A sharp and brief temperature increase of a NP generated by a femtosecond laser can also contribute to confine the temperature increase at the close vicinity of the NP to avoid extended heating of the whole medium when not desired.[16]

Several experimental and numerical approaches aimed at studying the internal processes of heat generation under pulsed illumination and the subsequent effects observed in the surrounding medium, e.g., temperature and pressure variations,[17–19] acoustic wave generation,[18] vibration modes,[20–22] cell apoptosis,[11] drug release[9,23] nanosurgery,[15,24] bubble formation,[25–28] NP shape modification[29] and melting,[29–31] nanosecond pulses for biomedical applications,[32,33] and extreme thermodynamics conditions.[33–37] However, to the best of our knowledge, there is still a lack of investigation regarding questions such as the temperature spatial extension in the surrounding medium or the efficiency compared to cw illumination. Some investigations have been carried out but are usually restricted to a particular NP geometry or using approximations such as a perfect interface conductivity. In other words, questions related to fs-pulsed heating of NPs have not been investigated in the whole space of parameters (size of the nanoparticle, interface conductivity, and illumination conditions). Such information is though fundamental since any experiment is characterized by different experimental conditions.

In this paper, we present and use a versatile numerical framework to investigate theoretically and numerically the evolution of the temperature distribution of a gold NP immersed in water when illuminated by a femtosecond-pulsed laser. We aim at providing a comprehensive description of the problem spanning the whole space of variables (NP size, interface conductivity, and illumination conditions). Various degrees of complexity exist to describe theoretically such a problem. We chose a progressive approach consisting in going from simple to more sophisticated considerations: We shall start with the more basic description of the problem, a pointlike source of heat to model the NP, and then refine the description of the system by taking into account successive refinements, namely, a finite-size structure, a gold-water interface conductivity, and a nonuniform NP inner temperature. In each case, the physics and the associated constitutive equations are detailed and the approximations discussed. The aim is to answer all the questions related to characteristic time, space, and temperature increase in fs-pulsed optical heating of a gold NP.

Details regarding the numerical algorithm we developed are given in the Appendix.

II. RESULTS AND DISCUSSION

A. Physical system

We consider a system with spherical symmetry consisting of a gold nanosphere of radius R immersed in water (Fig. 1). This nanoparticle is uniformly illuminated by a laser light at its plasmonic resonance angular frequency $\omega = 2\pi\, c_0/\lambda_0 = k\, c_0/n_w$, where c_0 is the speed of light and n_w is the optical index of water. No mass transfer such as fluid convection or bubble formation is considered. We shall focus on a moderate temperature increase (typically a few tens of degrees)

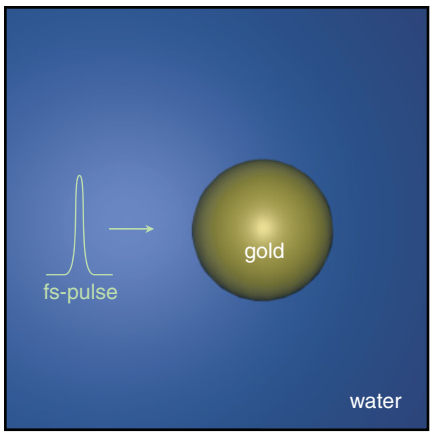

FIG. 1. (Color online) System investigated: A spherical gold NP immersed in water illuminated by a femtosecond-pulsed laser.

and do not consider extreme thermodynamic conditions. For this reason, all the parameters describing the materials (water and gold) are assumed to remain constant within the temperature range investigated. Whenever a femtosecond pulse is mentioned, it has to be understood as a pulse, the duration of which is smaller than the characteristic time of electron-phonon scattering $\tau_{\text{e-ph}} \sim 1.7$ ps. For instance, this can correspond to the use of a Ti:sapphire laser, which usually provides a pulse duration of ∼100 fs.

In the following, any mentioned temperature T stands for a temperature *increase* above this initial ambient temperature T_∞.

Anywhere in the system, we can define the thermal energy density and thermal current density that read, respectively, $u_{\text{th}}(r,t) = \rho\, c\, T(r,t)$ and $\mathbf{j}_{\text{th}}(r,t) = -\kappa \boldsymbol{\nabla} T(r,t)$ where ρ is the mass density, c is the specific heat capacity at constant pressure, and κ is the thermal conductivity of the system at the position r. From the energy conservation equation $\partial_t u_{\text{th}}(r,t) + \boldsymbol{\nabla} \cdot \mathbf{j}_{\text{th}}(r,t) = p(r,t)$, one obtains the heat diffusion equation

$$\rho c\, \partial_t T(r,t) = \kappa \nabla^2 T(r,t) + p(r,t) \tag{1}$$

where $p(r,t)$ is the heat power density [nonzero only inside the NP ($r < R$), where the light is absorbed].

For the system under consideration in this work, this yields a set of two differential equations, one for each medium (gold and water), along with two boundary conditions at the gold-water interface:

$$\begin{cases} \text{Diffusion equations:} \\ \rho_{\text{Au}} c_{\text{Au}}\, \partial_t T(r,t) = \kappa_{\text{Au}} \nabla^2 T(r,t) + p(r,t) \text{ for } r < R, \\ \rho_{\text{w}} c_{\text{w}}\, \partial_t T(r,t) = \kappa_{\text{w}} \nabla^2 T(r,t) \text{ for } r > R. \\ \text{Boundary conditions at } r = R: \\ \kappa_{\text{w}} \partial_r T(R^+,t) = \kappa_{\text{Au}} \partial_r T(R^-,t), \\ T(R^+,t) = T(R^-,t). \end{cases} \tag{2}$$

The Au and w subscripts refer to gold and water. The first boundary condition ensures heat flux conservation at the NP interface.

It has been demonstrated experimentally that an interface resistivity at the gold/water interface exists and can play a significant role in the heat release.[38–41] The interface resistivity can reach appreciable values when the liquid does not wet the solid. The wetting depends on the nature of the interface, and, in particular, a possible molecular coating. Namely, hydrophobic coatings are associated with poor thermal conductivities. The direct consequence of a finite interface conductivity g (or resistivity $1/g$) is a temperature drop/jump/discontinuity ΔT at the NP interface such that

$$\mathcal{P}(t) = 4\pi R^2 g\, \Delta T(t), \tag{3}$$

where ΔT is defined as

$$\Delta T(t) \equiv T(R^-,t) - T(R^+,t) \tag{4}$$

(in this work, the symbol $\equiv$ symbolizes a definition). The released heat power $\mathcal{P}(t)$ is also related to the temperature gradient on the NP surface through the energy conservation equation

$$\mathcal{P}(t) = -4\pi R^2 \kappa_{\text{w}}\, \partial_r T(R,t). \tag{5}$$

Equations (3) and (5) yield a modification of the second boundary condition of system (2) at the nanoparticle interface $r = R$:

$$-\partial_r T(R^+,t) = \frac{1}{l_{\text{K}}} \Delta T(t), \tag{6}$$

where $l_{\text{K}} = \kappa_{\text{w}}/g$ is named the Kapitza length and $1/g$ is the associated Kapitza resistivity.

Let us define from now the two dimensionless constants that we shall often use in the following,

$$\beta \equiv \frac{\rho_{\text{w}} c_{\text{w}}}{\rho_{\text{Au}} c_{\text{Au}}} \approx 1.680, \tag{7}$$

$$\gamma \equiv \frac{\kappa_{\text{Au}}}{\kappa_{\text{w}}} \approx 512, \tag{8}$$

and one dimensionless parameter

$$\lambda_{\text{K}} \equiv \frac{\kappa_{\text{w}}}{gR} = \frac{l_{\text{K}}}{R} \tag{9}$$

that is the Kapitza length normalized by the NP radius R. We also introduce dimensionless space ρ and time τ variables defined as

$$\rho \equiv r/R, \tag{10}$$

$$\tau \equiv a_{\text{w}} t/R^2, \tag{11}$$

where $a = \kappa/\rho c$ is called the thermal diffusivity. R and R^2/a_{w} are indeed the natural space and time units associated with the system. Within this work, we will make an extensive use of dimensionless variables and constants, first because it yields simpler, more natural formulas and more general results, and then because it shows how the algorithm can be properly written, i.e., working with numbers close to 1 and not unnecessary powers of 10. However, for the sake of simplicity, even when using normalized variables, we shall keep the same function names, e.g., $T(r,t)$ and $T(\rho,\tau)$. But this mathematical digression should not cause any clarity issue.

TABLE I. Physical constants used in this work associated with gold and water.[a]

Name	Gold	Water	Unit
Thermal conductivity κ	317	0.60	W/m/K
Specific heat capacity[b] c	129	4187	J/kg/K
Mass density ρ	19.32	1.00	$\times 10^3$ kg/m^3
Thermal diffusivity a	127	0.143	$\times 10^{-6}$ m^2/s

[a]Values at ~25 °C taken from Ref. 42.
[b]At constant pressure.

Using these dimensionless variables, parameters, and constants, the set of Eqs. (2) along with the additional boundary condition (6) read then

$$\begin{cases} \text{Diffusion equations:} \\ \partial_\tau T(\rho,\tau) = \frac{\gamma\beta}{\rho^2}\partial_\rho[\rho^2\partial_\rho T(\rho,\tau)] + p(\rho,\tau) \text{ for } \rho < 1, \\ \partial_\tau T(\rho,\tau) = \frac{1}{\rho^2}\partial_\rho[\rho^2\partial_\rho T(\rho,\tau)] \text{ for } \rho > 1. \\ \text{Boundary conditions at } \rho = 1: \\ \partial_\rho T(1^+,\tau) = \gamma\,\partial_\rho T(1^-,\tau) = -\frac{1}{\lambda_K}\Delta T(\tau), \end{cases} \tag{12}$$

where the Laplacian operator ∇^2 has been reformulated using spherical coordinates.

From now on, the use of a dimensionless formalism will not be systematic but preferred when it simplifies the notations and makes the results more general.

B. Numerical method

The set of Eq. (12) has no simple analytical solution. We chose to solve it numerically by developing a finite difference method (FDM) and a Runge-Kutta (RK) algorithm.[43] Basically, it is based on a spatiotemporal discretization of the system of Eqs. (12) according to

$$\begin{aligned} \rho_i &\equiv i \times \delta\rho, \quad i \in [0,N], \\ \tau_j &\equiv j \times \delta\tau, \quad j \in [0,M], \\ T_{i,j} &\equiv T(\rho_i,\tau_j), \\ \partial_\rho\, T(\rho,\tau) &\to \frac{T_{i+1,j} - T_{i,j}}{\delta\rho}, \\ \partial_\tau\, T(\rho,\tau) &\to \frac{T_{i,j+1} - T_{i,j}}{\delta\tau}. \end{aligned} \tag{13}$$

This discretization procedure is associated with a RK algorithm of the fourth order (RK4) that ensures a higher accuracy—compared to regular Euler algorithms of the first order—in the estimation of $T_{i,j}$ at each spatiotemporal step.

Further details regarding the numerical algorithm are given in the Appendix.

C. cw illumination

Before studying what occurs under fs-pulsed illumination, it is worth describing first what happens under cw illumination. We consider here a uniform cw illumination of irradiance I and wavelength λ_0.

Under cw illumination, the establishment of the steady-state temperature profile will be preceded by a transient evolution. By dimensional analysis of the two diffusion equations of system (2), one finds that two time scales come into play:

$$\tau_d^w = \frac{\rho_w c_w}{\kappa_w} R^2 = \frac{R^2}{a_w}, \tag{14}$$

$$\tau_d^{Au} = \frac{\rho_{Au} c_{Au}}{\kappa_{Au}} R^2 = \frac{R^2}{a_{Au}}. \tag{15}$$

τ_d^w is the characteristic time associated with the evolution of the temperature profile in the surrounding water while τ_d^{Au} characterizes the temperature evolution inside the gold NP. Since $a_{Au} \gg a_w$, the thermalization inside the NP occurs much faster. Consequently, one can consider that the global establishment of the temperature profile of the overall system is governed by the time scale τ_d^w.

We consider now the final steady-state regime. The set of equations now reads

$$\begin{cases} \kappa_{Au}\nabla^2 T(r) = -p(r) \quad \text{for } r < R, \\ \kappa_w \nabla^2 T(r) = 0 \quad \text{for } r > R, \\ \kappa_w \partial_r T(R^+) = \kappa_{Au}\partial_r T(R^-) \\ \quad = -g\,\Delta T, \end{cases} \tag{16}$$

where $\Delta T \equiv T(R^-) - T(R^+)$. If one considers an average power density $p_0 = \mathcal{P}_0/V$, the solution has a simple form and reads

$$T^{cw}(r) = \frac{\mathcal{P}_0}{4\pi\kappa_w r} \quad \text{for } r > R, \tag{17}$$

$$T^{cw}(r) = \frac{\mathcal{P}_0}{4\pi\kappa_w R}\left[1 + \frac{1}{2\gamma}\left(1 - \frac{r^2}{R^2}\right) + \lambda_K\right] \quad \text{for } r < R, \tag{18}$$

where $\mathcal{P}_0$ is the heat power dissipated in the NP. Note that the temperature profile outside the NP does not depend on the NP surface conductivity.[44] Since $\gamma \gg 1$, one can usually consider—whatever the NP size—that the inner temperature of the NP is uniform and equals

$$T_{NP}^{cw} = \frac{\mathcal{P}_0}{4\pi\kappa_w R}(1 + \lambda_K) = \frac{\sigma_{abs} I}{4\pi\kappa_w R}(1 + \lambda_K), \tag{19}$$

where σ_{abs} is the optical absorption cross section of the NP.[2,45] For spherical nanoparticle smaller than $2R \sim 30$ nm, a good approximation can be used:[46,47]

$$\sigma_{abs} = k\,\mathrm{Im}(\alpha) - \frac{k^4}{6\pi}|\alpha|^2, \tag{20}$$

where

$$\alpha = 4\pi R^3 \frac{\varepsilon_{Au} - \varepsilon_w}{\varepsilon_{Au} + 2\varepsilon_w}, \tag{21}$$

with ε_{Au} the gold permittivity and ε_w the water permittivity.

From Eq. (19), we obtain a simple and very useful formula that gives the steady-state temperature of small spherical NP ($R < 15$ nm) under cw illumination:

$$T_{NP}^{cw} = \frac{k I R^2}{\kappa_w}\mathrm{Im}\left(\frac{\varepsilon_{Au} - \varepsilon_w}{\varepsilon_{Au} + 2\varepsilon_w}\right), \tag{22}$$

$$T_{NP}^{cw} \approx 2.00\frac{k I R^2}{\kappa_w}. \tag{23}$$

The latter formula applies for $\lambda_0 = 520$ nm. No interface resistivity is assumed in this formula ($\lambda_K = 0$). If the NP is not necessarily smaller than $2R = 30$ nm, the previous formalism becomes inappropriate and the more sophisticated and general Mie theory has to be used.[46,47] Within this model, the absorption cross section reads

$$\sigma_{abs} = \frac{2\pi}{k^2}\sum_{j=1}^{\infty}(2j+1)(|a_j|^2 + |b_j|^2),$$

where

$$a_j = \frac{m\psi_j(w)\psi_j'(v) - \psi_j(v)\psi_j'(w)}{m\psi_j(w)\xi_j'(v) - \xi_j(v)\psi_j'(w)},$$

$$b_j = \frac{\psi_j(w)\psi_j'(v) - m\psi_j(v)\psi_j'(w)}{\psi_j(w)\xi_j'(v) - m\xi_j(v)\psi_j'(w)},$$

and $m^2 = \varepsilon_{Au}/\varepsilon_w$, $v = kR$, and $w = mv$. The primes indicates differentiation with respect to the argument in parentheses. ψ_j and ξ_j are Ricatti-Bessel functions defined as

$$\psi_j(x) = \sqrt{\frac{\pi x}{2}}J_{j+\frac{1}{2}}(x),$$

$$\xi_j(x) = \sqrt{\frac{\pi x}{2}}\left[J_{j+\frac{1}{2}}(x) + iY_{j+\frac{1}{2}}(x)\right].$$

J_ν and Y_ν are the Bessel functions of first and second order, respectively. The derivatives can be expressed as follows:

$$\psi_j'(x) = \psi_{j-1}(x) - \frac{j}{x}\psi_j(x),$$

$$\xi_j'(x) = \xi_{j-1}(x) - \frac{j}{x}\xi_j(x).$$

In the following, the Mie theory will be used whenever a calculation of the absorption cross section is required.

D. Pulsed illumination and initial temperature increase

We consider now a fs-pulsed illumination of average irradiance $\langle I\rangle$, pulse repetition rate f, fluence $F = \langle I\rangle/f$, and wavelength λ_0.

The absorption of a fs pulse by a metal nanoparticle can be described as a three-step process[48,49] that involves different time scales:

1. Electronic absorption. During the interaction with the fs pulse, part of the incident pulse energy is absorbed by the gas of free electrons of the NP, much lighter and reactive than the ions of the lattice. The electronic gas thermalizes very fast to a Fermi-Dirac distribution over a time scale $\tau_e \sim 100$ fs.[49] This leads to a state of nonequilibrium within the NP: The electronic temperature T_e of the electronic gas has increased while the temperature of the lattice (phonons) T_p remains unchanged. The absorbed energy $\mathcal{E}_0$ reads

$$\mathcal{E}_0 = \sigma_{abs}\langle I\rangle/f = \sigma_{abs}F = \mathcal{P}_0/f. \quad (24)$$

2. Electron-phonon thermalization. Subsequently this hot electronic gas relaxes (cools down), through internal electron-phonon interaction characterized by a time scale $\tau_{e\text{-}ph}$ to thermalize with the ions of the gold lattice. This time scale is not dependent on the size of the NP except for NP smaller than 5 nm due to confinement effects.[50] For a larger NP and for moderate pulse energy, the time scale is constant and equals $\tau_{e\text{-}ph} \sim 1.7$ ps.[51–53] At this point, the NP is in internal equilibrium at a uniform temperature ($T_e = T_p$), but is not in equilibrium with the surrounding medium that is still at the initial ambient temperature.

3. External heat diffusion. The energy diffusion to the surroundings usually occurs at higher characteristic time scale τ_d, which leads to a cooling of the NP and a heating of the surrounding liquid. The time scale of this process depends on the size of the NP and ranges from 100 ps to a few ns. For small NP (<20 nm), this third step can overlap in time with the electron-phonon thermalization[19] (as discussed hereafter).

If one considers that the electron-phonon thermalization (step 2) occurs much faster than the external heat diffusion (step 3), the NP temperature reaches an initial maximum temperature T_{NP}^0 that is straightforward to estimate by energy consideration. It is related to the absorbed energy through the relation

$$\mathcal{E}_0 = V\rho_{Au}c_{Au}T_{NP}^0, \quad (25)$$

where V is the volume of the NP and $V\rho_{Au}c_{Au}$ is its heat capacity. Using Eq. (24), we find that the maximum initial NP temperature is

$$T_{NP}^0 = \frac{\sigma_{abs}F}{V\rho_{Au}c_{Au}}. \quad (26)$$

This formula is not restricted to spherical nanoparticles. As an example, for a gold nanorod, 50 nm long and 12 nm in diameter, at the plasmonic resonance ($\lambda_0 = 800$ nm), considering a random orientation $f = 86$ MHz and $\langle I\rangle = 1.0$ mW/μm^2, we obtain $T_{NP}^0 \approx 30\,^\circ$C. Note that for a given laser power, the temperature increase does not depend on the pulse duration, but only on the pulse energy $\langle I\rangle/f$.

It is worth comparing the instantaneous temperature increase T_{NP}^0 after a single fs pulse and the steady-state temperature T_{NP}^{cw} achieved under cw illumination. From Eqs. (19) and (26), we obtain a dimensionless number η_0 that quantifies the gain obtained when using pulsed illumination:

$$\eta_0 \equiv \frac{T_{NP}^0}{T_{NP}^{cw}} = \frac{3\beta a_w}{fR^2(1+\lambda_K)}. \quad (27)$$

Figure 2 illustrates what η_0, T_{NP}^0, and T_{NP}^{cw} represent for a particular example. This useful formula is only valid for large values of η_0. When R or f tends to be high, successive pulses may overlap (as explained later in Sec. II H), which makes the assumption of a single-pulse illumination wrong. Furthermore, for very small particles, a temperature damping effect occurs (by a typical factor 2) and T_{NP}^0 is not the initial temperature, as explained hereafter. Consequently, this formula is a good approximation of the temperature gain achieved under fs-pulsed illumination compared to cw illumination as far as η_0 remains large and the NP radius not too small ($R > 10$ nm). The true values of η_0, i.e. whatever the NP radius R and surface conductivity g and without approximations, is numerically computed and discussed in Sec. II G.

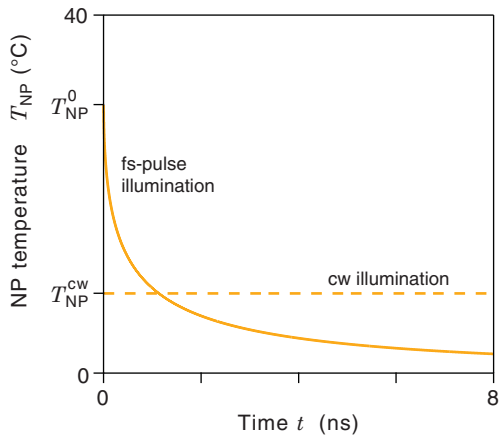

FIG. 2. (Color online) Evolution of the temperature of a NP with a radius $R = 50$ nm under cw illumination (dashed line) and after a single-pulse illumination (solid line) for a given irradiance $\langle I \rangle = 0.1\ \mathrm{mW}/\mu\mathrm{m}^2$. This figure aims at visually defining the initial temperature increase T^0_{NP} under pulsed illumination and the steady-state temperature T^{cw}_{NP} under cw illumination. For this particular case, $T^0_{NP} = 31\,^\circ\mathrm{C}$ while $T^{cw}_{NP} = 9.2\,^\circ\mathrm{C}$.

E. Subsequent evolution of the temperature profile

We discuss now the subsequent evolution of the temperature field $T(r,t)$ after a single-pulse illumination, i.e., after an initial temperature increase T^0_{NP}.

In the ideal case consisting of a pointlike NP ($R \to 0$), the heat power density can be described by a Dirac distribution

$$\rho_w c_w\, \partial_t T(r,t) = \kappa_w \nabla^2 T(r,t) + \mathcal{E}_0 \delta(\mathbf{r})\delta(t). \tag{28}$$

This ideal problem has a simple analytical solution that reads

$$T(r,t) = \frac{\mathcal{E}_0}{c_w \rho_w} \frac{1}{(4\pi a_w t)^{3/2}} \exp\left(-\frac{r^2}{4\pi a_w t}\right). \tag{29}$$

Then, the *envelope* $T_{max}(r) \equiv \max_t[T(r,t)]$ of the temperature profile over time can be easily obtained by using formula (29) and calculating the time t for which $\partial_t T(r,t) = 0$ for any position r. It yields a temperature envelope

$$T_{max}(r) = \frac{1}{3\sqrt{3}} \frac{\mathcal{E}_0}{c_w \rho_w} \frac{1}{r^3}.$$

Interestingly, the temperature profile under pulsed illumination follows a $1/r^3$ spatial decrease, which makes a real difference compared to continuous illumination characterized by a steady-state profile of $1/r$ [see Eq. (17)]. This is a first clue that pulsed illumination achieves a much higher-temperature confinement around the NP.

We consider now the more general and realistic case of a spherical NP defined by a finite radius $R \neq 0$. In this case, no simple analytical solution exists but some approximations can be done. First, the initial temperature profile $T(r,0)$ can be considered as uniform (equals T^0_{NP}) inside the NP since the electron-phonon thermalization usually occurs much faster than the external heat diffusion. Then, one can also suppose that the NP temperature *remains* uniform during the evolution of the system since $\kappa_{Au} \gg \kappa_w$. Hence,

$$\forall t, \quad T(r,t) = T_{NP}(t) \quad \text{for } r < R. \tag{30}$$

The validity of these two approximations will be investigated and discussed in more detail in Sec. II G. Under these assumptions, the system of Eq. (2) can be simplified:

$$\begin{cases} \text{Diffusion equation:} \\ \rho_w c_w \partial_t T(r,t) = \kappa_w \frac{1}{r^2} \partial_r t[r^2\, \partial_r T(r,t)] \quad \text{for } r > R. \\ \text{Boundary conditions:} \\ V \rho_{Au} c_{Au} \frac{dT_{NP}(t)}{dt} = \kappa_w 4\pi R^2 \partial_r T(R,t) = -g 4\pi R^2 \Delta T(t). \end{cases} \tag{31}$$

The first equation is the heat diffusion equation outside the NP. The two other equations come from considerations of energy conservation and will control the boundary condition at the NP interface ($r = R$).

Interestingly, two new characteristic times arise from the boundary equations. They read

$$\tau_d^{NP} = R^2 \frac{\rho_{Au} c_{Au}}{3\kappa_w}, \tag{32}$$

$$\tau_d^{s} = \frac{R \rho_{Au} c_{Au}}{3g}. \tag{33}$$

These characteristic times are associated to the evolution of the nanoparticle average temperature, i.e., the heat energy stored in the NP. When the surface resistivity $1/g$ is high (respectively small), the evolution is governed by τ_d^s (respectively τ_d^{NP}). These new time scales differ from τ_d^{Au} and τ_d^w that were respectively the characteristic times associated to the establishment of the internal temperature equilibrium inside the NP and the temperature diffusion outside the NP. If the surface conductivity g is small enough, the evolution of the NP temperature is governed by τ_d^s. If the surface resistivity is negligible, the evolution is governed by τ_d^{NP}. The temperature evolution inside and outside the NP is thus governed by a subtle interplay between four time scales. Three of them are linked by the relation

$$\tau_d^w = \gamma\beta \tau_d^{Au} = 3\beta \tau_d^{NP}, \tag{34}$$

which yields

$$\tau_d^w \approx \tau_d^{NP} \gg \beta \tau_d^{Au}. \tag{35}$$

Regarding the fourth time scale τ_d^s, it can be dominant or negligible depending on the values of R and g.

Using dimensionless time τ and space ρ variables, the system of equations (31) can be recast into this simpler form:

$$\begin{cases} \text{Diffusion equation:} \\ \partial_\tau T(\rho,\tau) = \frac{1}{\rho^2} \partial_\rho [\rho^2\, \partial_\rho T(\rho,\tau)] \quad \text{for } \rho > 1. \\ \text{Boundary conditions:} \\ \frac{dT_{NP}(\tau)}{d\tau} = 3\beta\, \partial_\rho T(1,\tau) = -\frac{3\beta}{\lambda_K} \Delta T(\tau), \end{cases} \tag{36}$$

where $\Delta T(\tau) = T_{NP}(\tau) - T(1,\tau)$.

Using the RK4 algorithm, system (36) was resolved numerically. The discretization parameters are $(\delta\rho, \delta\tau, N, M) = (15 \times 10^{-3}, 4 \times 10^{-6}, 400, 10^6)$. The interface resistivity $1/g$ was set to zero (nonzero values are discussed in the next section). The result is presented in Fig. 3 that displays the universal normalized evolution of the temperature of a NP. This profile applies for any particle size since it uses the normalized variables (ρ,τ): For a given particle size R, the

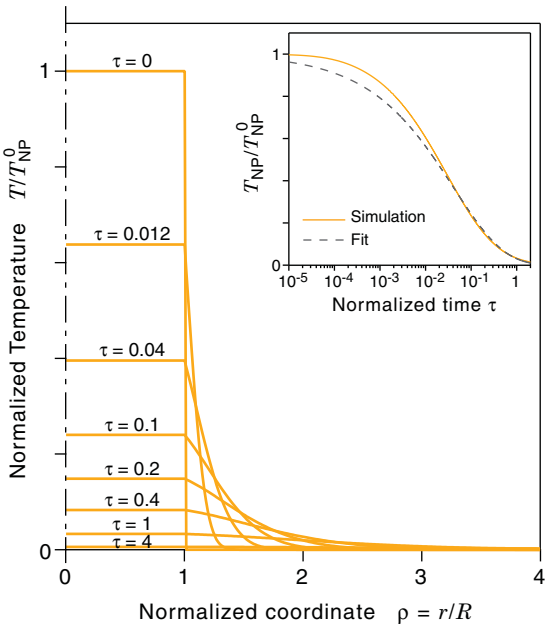

FIG. 3. (Color online) Result of a numerical simulation showing the universal evolution of the temperature profile for a NP of radius R at different normalized time $\tau = a_w t/R^2$. No interface resistivity is considered ($1/g = 0$). The inset shows the evolution of the NP inner temperature as function of time.

normalized coordinate ρ has to be multiplied by R and the normalized time τ by R^2/a_w to recover the actual coordinate r and time t. Hu and Hartland[19] have shown experimentally that the NP temperature can be conveniently fitted using a stretched exponential function

$$F(\tau) = e^{-(\tau/\tau_0)^n}. \tag{37}$$

We used this function to fit the evolution of the NP temperature as represented in the inset of Fig. 3 (dashed line). The optimized fit parameters are $n = 0.39$ and $\tau_0 = 0.041$. This yields a useful formula giving the normalized NP inner temperature evolution for any particle radius R:

$$F_R(t) = \exp\left[-\left(\frac{a_w t}{0.041 R^2}\right)^{0.39}\right]. \tag{38}$$

Note that this useful formula assumes a zero interface resistivity $1/g$. For a finite value of g, the values of the fit parameters τ_0 and n are different and have to be recalculated using the FDM.

Figure 4 aims at comparing the temperature profiles under pulsed and cw illuminations. It replots the series of temperature profiles of Fig. 3 along with the temperature envelope and the temperature profile of the steady state (cw illumination) given by Eq. (17). As derived in the previous section, when considering a pointlike ($R \to 0$) source of heat, the envelope of the temperature profile follows a $1/r^3$ profile outside the NP. When considering now a finite-size NP, it appears that such a simple law does not exist. Instead, a stretched exponential

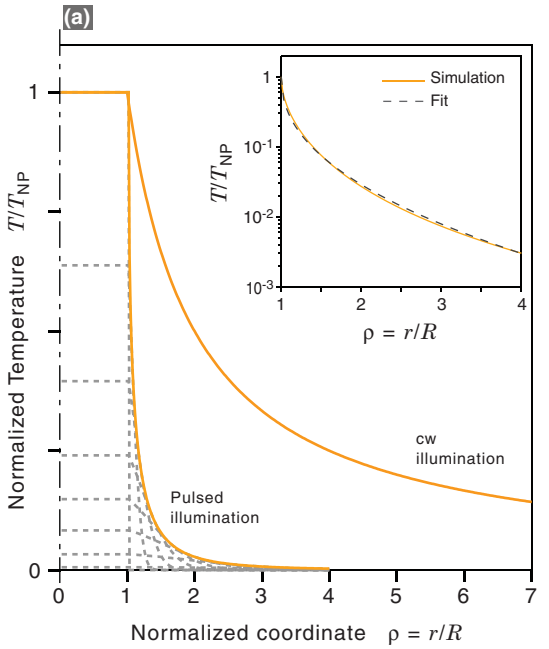

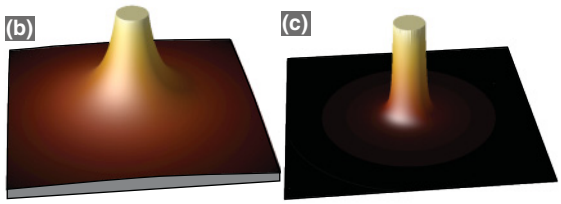

FIG. 4. (Color online) (a) Comparison between the steady-state temperature profile under cw illumination and the envelope of the temperature evolution under pulsed illumination. The inset shows the fit of the NP temperature profile in the case of a pulsed illumination. (b) Temperature profile around the NP under cw illumination. (c) Envelope of the temperature profile over time around the NP subsequent to a fs-pulse illumination.

function can also be conveniently used to fit the envelope of the spatial temperature profile in the surrounding water:

$$F(\rho) = \exp\left[-\left(\frac{\rho - 1}{\rho_0}\right)^n\right]. \tag{39}$$

The fit parameters are $n = 0.45$ and $\rho_0 = 0.060$. These results illustrate to what extent pulsed illumination achieves a much higher degree of temperature confinement compared to cw illumination.

Note that the evolution of the system is characterized by an energy conservation law. At any time t, the energy of the system is constant and reads

$$\mathcal{E}_0 = \frac{4}{3}\pi R^3 \rho_{Au} c_{Au} T_{NP}(t) + \int_R^\infty \rho_w c_w 4\pi r^2 T(r,t) dr, \tag{40}$$

or using the normalized variables and constants defined above, the normalized energy reads

$$\epsilon_0 = \frac{T_{NP}(\tau)}{T^0_{NP}} + \int_1^\infty 3\beta\rho^2 \frac{T(\rho,\tau)}{T^0_{NP}} d\rho = 1. \tag{41}$$

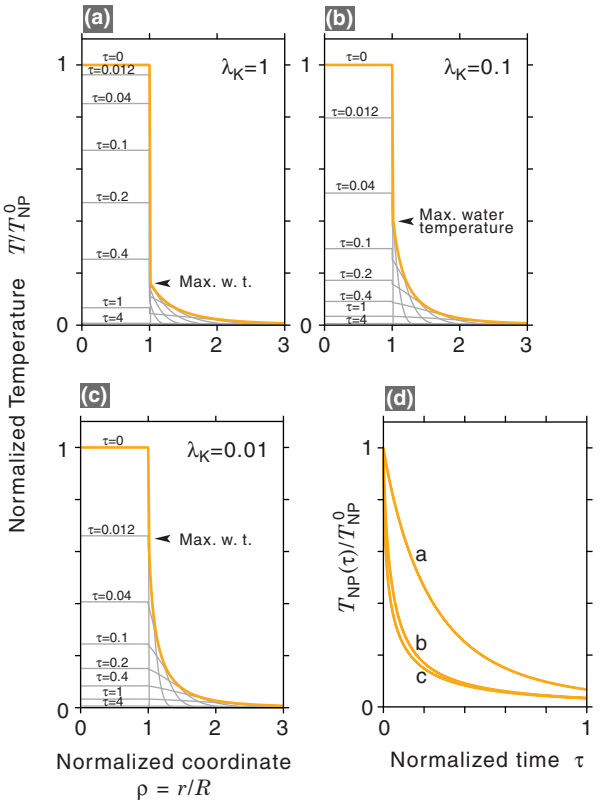

FIG. 5. (Color online) (a)–(c) Temperature envelope of the temperature evolution for three different values of normalized Kapitza length λ_K. Temperature profiles are also represented at different times (in gray). (d) Evolution of the NP inner temperature corresponding to the three previous situations.

This conservation law can be conveniently used in numerical simulations as a verification of the consistency of the result. For example, in the simulations shown in Fig. 3, it varied by less than 0.2%.

F. Finite conductivity of the gold-water interface

In this section, we shall go one step further into the refinement of the analytical description of the problem. We still consider the NP temperature as uniform, but we take into account a finite interface conductivity g. The set of equations describing the system is given by (36). Figure 5 displays the evolution of the temperature profiles for a set of different normalized Kapitza length (i.e., gold/water interface conductivity). Usual values of the interface conductivity g range from 50 to ∞ MW/(m^{2}K).[38,41,54] As an example, gold nanorods coated with cetyltrimethylammonium bromide (CTAB) molecules are endowed with a typical surface conductivity of 130 MW/(m^{2}K).[38] For NP radii ranging from 5 to 50 nm, typical normalized Kapitza lengths λ_K are thus ranging from $\sim$0 to 2.

For a large Kapitza length (high interface resistivity), the heating of the surrounding fluid can be highly inefficient as observed in Fig. 5(a). This is due to the fact that the high resistivity of the NP interface tends to slow down the heat release, which yields a weaker maximum temperature in water. The same amount of energy is released in the surroundings but more slowly.

G. Beyond the approximation of instantaneous temperature increase

In the previous section, we used two approximations regarding the NP temperature to simplify the problem.

First, we considered that the NP temperature increase $T^0_{\rm NP}$ subsequent to the pulse of light was instantaneous and uniform inside the NP. This was because the characteristic time of electron-phonon scattering ($\tau_{\text{e-ph}} \sim 1.7$ ps) is usually shorter than the diffusion time into the surrounding [see Eq. (32)], but this may become nonvalid for small NPs.

Second, we assumed that the NP temperature remained uniform inside the NP during the overall evolution. That was because the thermal conductivity of gold is much larger than the one of water.

Yet, the validity of these two approximations may depend *a priori* on the size R and the interface conductivity g of the NP. The numerical algorithm used in this work allows one to consider the inner temperature of the NP as not necessarily uniform and to investigate the step where the temperature increases while the NP is being illuminated by the pulse. We can thus investigate the validity of the two approximations mentioned above by simulating the evolution of the inner temperature profile, both during the electron-phonon thermalization and during the subsequent heat diffusion in the surrounding medium. This is the purpose of this section.

During the electron-phonon thermalization, one can assume that the heat power density $p(r,t)$ is uniform all over the NP:

$$p(r,t) = p_0(t) = \frac{\mathcal{E}_0}{V\tau_{\text{e-ph}}}\exp(-t/\tau_{\text{e-ph}}). \tag{42}$$

Indeed, we have seen in Sec. II D that the electronic thermalization (step 1) occurs much faster than the energy transfer from the electrons to the lattice (step 2). The heating of the lattice is thus performed by a uniformly hot electronic gas. The dimensionless form reads

$$p_0(\tau) = T^0_{\rm NP}\frac{\tau_{\rm p}^{\rm w}}{\tau_{\text{e-ph}}}\exp\left(-\tau\tau_{\rm p}^{\rm w}/\tau_{\text{e-ph}}\right).$$

Note that under cw illumination, the heat generation density is on the contrary highly nonuniform within the NP.[55]

Within this other approach characterized by an initial zero temperature profile and a heat power density in the NP, the energy conservation law now reads, at any normalized time τ, under cw illumination,

$$3\beta T^{\rm cw}_{\rm NP}\tau = \int_0^1 3\rho^2 T(\rho,\tau)d\rho + \int_1^\infty 3\rho^2\beta T(\rho,\tau)d\rho, \tag{43}$$

and under pulsed illumination,

$$T^0_{\rm NP}\left[1-\exp\left(\frac{-\tau\tau_{\rm d}^{\rm w}}{\tau_{\text{e-ph}}}\right)\right] = \int_0^1 3\rho^2 T(\rho,\tau)d\rho + \int_1^\infty 3\rho^2\beta T(\rho,\tau)d\rho. \tag{44}$$

Figure 6 presents the results of the numerical simulations for two NP sizes $R = 5$ and $R = 50$ nm, and for $1/g = 0$. It

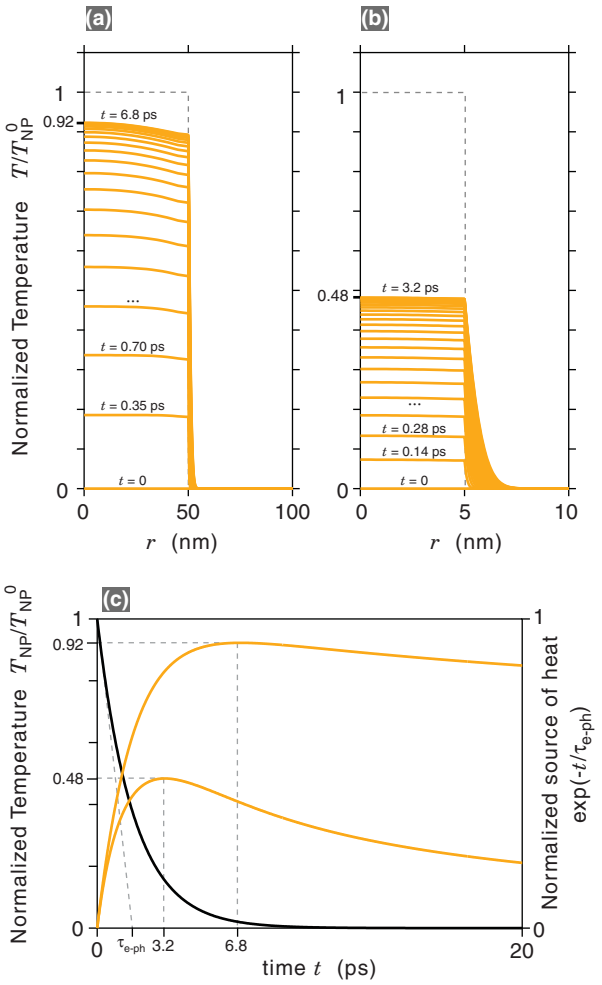

FIG. 6. (Color online) Temperature rise subsequent to a femtosecond-pulsed illumination for a NP 100 nm in diameter (a) and 10 nm in diameter (b) (interface resistivity $1/g = 0$). The ideal temperature profile that the NP would achieve if there were no heat release in the surrounding is represented by a dashed line. (c) Evolution of the temperature $T(r = 0,t)$ for the two above-mentioned cases along with the normalized heat power $p_0(t)$ (dark line) delivered by the excited electronic gas to the phonons. The normalized temperature does not reach 1 due to heat release during the NP heating.

shows the temperature evolution during the heating phase from the initial zero uniform temperature *up to the time when the NP temperature reaches its maximum value*. We can see that when considering a possible heat leak into the surrounding during the pulse illumination, the NP temperature does not reach necessarily T^0_{NP}. For large NP, the inner temperature profile suffers from some distortion when the temperature reaches its highest value [Fig. 6(a)]. However, the maximum temperature reaches practically the ideal maximum temperature T^0_{NP}. Indeed, one can see that the heat diffusion into the surroundings is almost absent. For a small NP [Fig. 6(b)], the temperature diffusion into the surrounding medium during this initial step is much more visible. The direct consequence is that the NP temperature does not reach its maximum ideal value T^0_{NP}, represented by dashed line in Fig. 6(b). The evolution of the NP inner temperature $[T(r = 0,t)]$ for the two above-mentioned cases ($R = 5$ and $R = 50$ nm) is plotted in Fig. 6(c). The temperature profiles are displayed along with the evolution of the heat power $p_0(t)$ provided by the free electron gas. For small particles, it is clear that the time scale $\tau_{e\text{-}ph}$ becomes of the same magnitude as the characteristic time of the heat diffusion in the surrounding. This explains why the NP temperature cannot reach the maximum ideal temperature T^0_{NP}. Note that the temperature T^0_{NP} used to normalize the curves in Fig. 6 depends on R [cf. Eq. (26)] and is thus not the same for the two cases.

In any case, the temperature remains quasiuniform inside the NP, which validates the usual assumption (30).

The maximum temperature achieved in the system is discussed in more detail in Fig. 7. Temperatures are plotted as function of NP size R and interface conductivity g. Figures 7(a) and 7(b) represent the maximum temperature *inside* and *outside* the NP:

$$T^{max}_{NP} = \max_t [T(r = 0,t)], \tag{45}$$

$$T^{max}(R^+) = \max_t [T(r = R^+,t)], \tag{46}$$

normalized by the ideal temperature increase T^0_{NP} [Eq. (26) and Fig. 7(g)]. When $T^{max}_{NP}/T^0_{NP} \ll 1$, it means that the heat release outside the NP is too fast. The characteristic time τ^w_d [Eq. (14)] becomes close to the characteristic time of the inner thermalization and steps 2 and 3 occur almost simultaneously. This happens when the particle is too small and when the surface conductivity is not weak. When $T^{max}_w/T^0_{NP} \ll 1$, it means that the water temperature increase is not optimum. This happens when the NP is too small, or when g is too small, giving rise to a large temperature drop at the NP interface.

Figures 7(c) and 7(d) represent the maximum temperature inside and outside the NP for a given irradiance $I = 0.1\ \mathrm{mW}/\mu\mathrm{m}^2$. Interestingly, we evidence an optimal NP size. NPs at approximately $2R = 40$ nm turn out to be the most efficient nanosource of heat for a given laser irradiance. Below this size, the cooling of the NP is too fast and the temperature has no time to reach T^0_{NP}, as explained above. Above this size, the absorption cross section is no longer proportional to the volume of the nanoparticle, as seen in Fig. 7(f) and in Eq. (20), which tends to damp the temperature increase. This trend is also observed in Fig. 7(d), which plots the associated temperature increase at the vicinity of the NP under the same illumination conditions. Moreover, we can see that to achieve a high-temperature increase inside (respectively outside) the NP, a low (respectively high) surface conductivity g is preferred.

Figure 7(e) aims at comparing the efficiency of pulsed versus cw illumination. In Eq. (2), we defined the gain η_0 with the approximation of an instantaneous temperature increase and no interface resistivity. Now we can define the exact gain η that takes into account the initial temperature damping and a finite interface conductivity:

$$\eta = T^{max}(R^+)/T^{cw}(R^+). \tag{47}$$

We observe that for small NPs and high surface conductivity [upper left-hand corner of Fig. 7(e)], a fs-pulsed illumination achieves a temperature rise of two orders of magnitude higher than cw illumination of the same average irradiance. However, depending on the NP size and surface conductivity, a pulsed

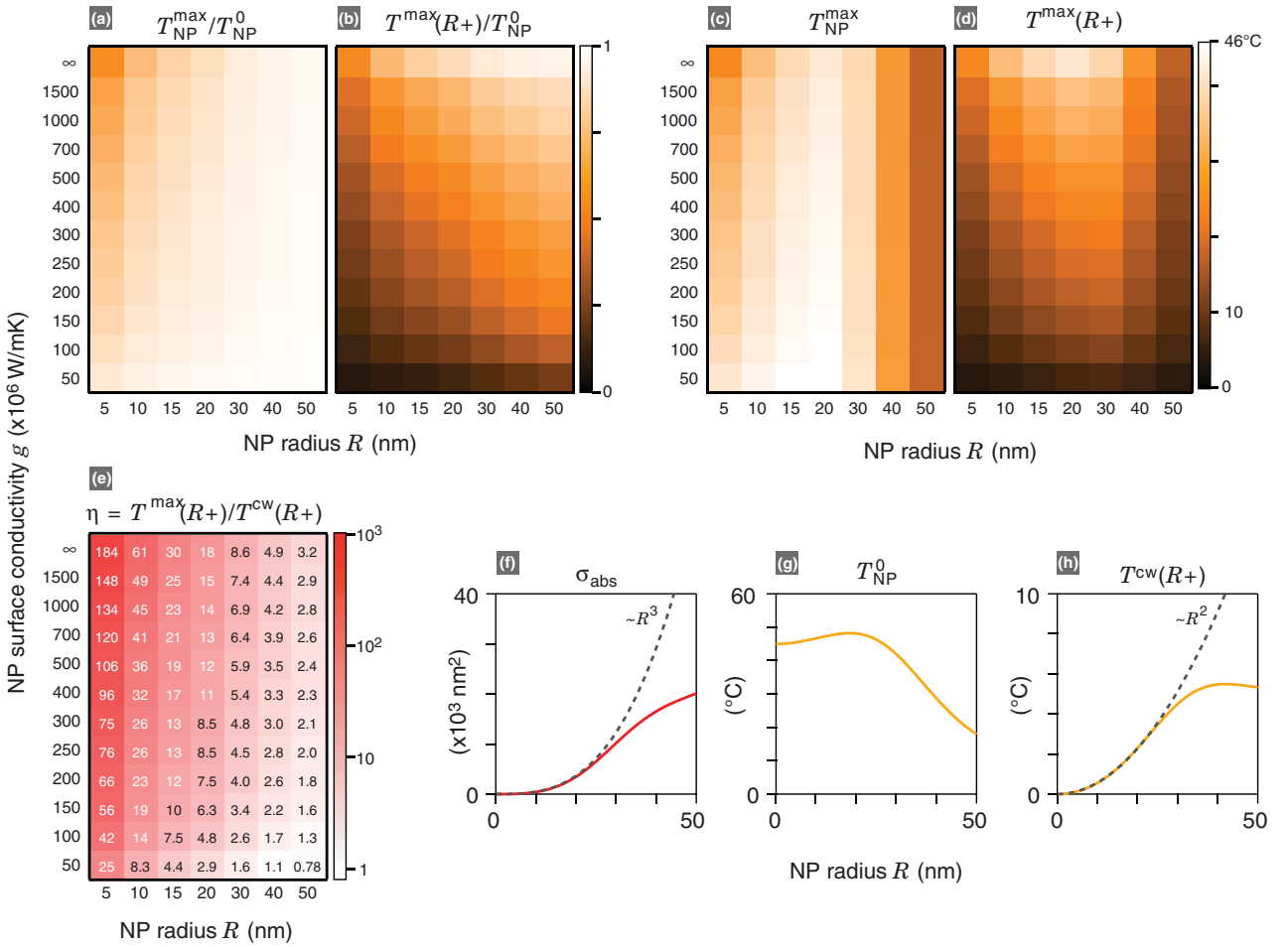

FIG. 7. (Color online) (a) Numerical calculations of the temperature maximum of the NP normalized by the ideal temperature increase T_{NP}^{0} for a set of different NP radii and surface conductivities. (b) Numerical calculations of the temperature maximum achieved in the surrounding medium normalized by the ideal temperature increase T_{NP}^{0}. (c) NP maximum temperature when illuminated by a pulsed laser, at a pulse repetition rate $f = 86$ MHz and an irradiance $I = 0.1$ mW/μm^2. (d) Maximum temperature of the surrounding medium under the same illumination conditions. (e) Ratio between the maximum temperature on the NP surface achieved *under pulsed illumination* and the temperature on the NP surface *under cw illumination* [Eq. (17)]. (f) Absorption cross section of a spherical gold NP as function of radius obtained from Mie theory [Eq. (24)] (solid line). The deviation from the R^3 law is represented by a dashed line. (g) Ideal temperature increase T_{NP}^{0} as function of NP radius. (h) Temperature on the NP surface under cw illumination [calculated from Eq. (17)]. The deviation from the R^2 law [see Eq. (23)] is represented by a dashed line.

illumination does not necessarily achieve a more pronounced temperature increase in the surrounding medium. Namely, for large NP of approximately $2R = 100$ nm in diameter, it appears that the use of pulsed illumination becomes inefficient since the gain in temperature reaches a maximum value of ~3. For low surface resistivity, the surrounding maximum temperature can even be higher when using cw illumination [lower right-hand corner of Fig. 7(e)]. Consequently, the use of a fs-pulsed laser is not necessarily efficient if one wants to achieve the highest temperature possible for a given laser power. This result questions the usefulness of fs-pulse illumination on lithographic structures, since it is usually larger than 100 nm.

H. Influence of the pulse repetition rate

When the relaxation time of the system is sufficiently long, the temperature of the NP has no time to return to zero between two successive pulses. This effect has not been considered so far and is the purpose of this section. The parameter that controls the appearance of such a regime is

$$\xi \equiv f\tau_d = f\left(\tau_d^{NP} + \tau_d^{s}\right) = fR^2\frac{\rho_{Au}c_{Au}}{\kappa_w}(1+\lambda_K). \quad (48)$$

Let $G_{R,g}(t)$ be the NP temperature evolution after a single-pulse illumination for a NP of radius R and interface conductivity g. Note that a fit formula of $G_{R,\infty}(t)$ for $g \to \infty$, assuming a top-hat initial temperature profile, is given by Eq. (38). Due to the linearity of all the equations governing the heat release and diffusion in the system, the NP temperature at any time t after a series of N pulses at the repetition rate f is

$$T_{NP}(t) = \sum_{j=0}^{N-1} G_{R,g}(t - j/f). \quad (49)$$

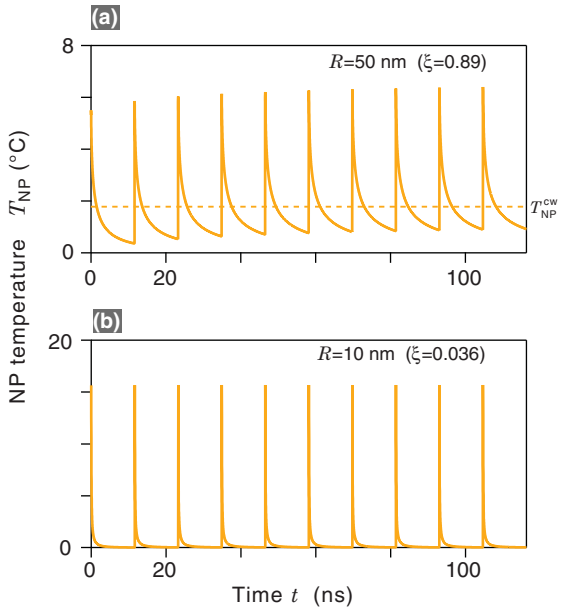

FIG. 8. (Color online) NP temperature during a series of ten pulses, $f = 86$ MHz, $\langle I \rangle = 1$ mW/μm^2, for a NP radius $R = 50$ nm (a) and $R = 10$ nm (b). In (a), the NP temperature corresponding to a cw illumination is $T_{NP}^{cw} = 1.78\,^{\circ}$C and is represented by a dashed line. In the second case, the NP temperature under cw illumination is $T_{NP}^{cw} = 0.30\,^{\circ}$C (not represented).

Figure 8 plots the results of numerical simulations for two cases corresponding to two different NP radii. The interface resistivity $1/g$ is assumed to be equal to zero. For a radius of $R = 50$ nm [Fig. 8(a)], ξ is close to unity, which yields a temperature offset: The NP temperature has no time to return to zero between two successive pulses. For even larger NPs, the temperature evolution would be even more smoothed and would tend to T_{NP}^{cw}. For weaker values of ξ, as shown in Fig. 8(b), the successive temperature pulses do not overlap and a regime of *time localization* can be achieved.

I. Extension to nonspherical nanoparticles

The numerical technique we have developed could be extended to two-dimensional (2D) systems modeling a NP with axial symmetry, such as nanorods. It would require a 2D mesh and longer computation times. However, most of the results presented in this work can be easily extended to nonspherical NPs without carrying out more sophisticated calculations: While the optical properties of NP particles depend very sensitively on the NP geometry—in particular, the resonance frequency—thermal processes of NP are only slightly dependent on the geometry.[2] For nonspherical NPs, we can define an effective radius R_{eff} such that the NP volume equals

$$V = \frac{4}{3}\pi R_{eff}^3. \tag{50}$$

Most of the reasonings we have done are also valid when replacing R by this effective radius R_{eff}.[2] In particular, Eq. (26) giving the ideal temperature increase T_{NP}^0 remains exact whatever the shape of the NP using R_{eff}. For gold nanorods, large aspect ratios would tend to make the cooling of the NP slightly faster by increasing the surface-to-volume ratio. However, all the orders of magnitude of time and space will remain identical as long as the aspect ratio remains moderate (less than $\sim$4).

III. SUMMARY AND CONCLUSION

To summarize, we have developed a versatile and yet simple numerical framework to investigate femtosecond-pulsed optical heating of spherical gold nanoparticles (NPs). This approach enabled us to address different models, from simple to more sophisticated, and to discuss the validity of their approximations. Most of the reasonings and calculations are made using dimensionless variables, parameters, and constants, which enabled us to compute universal behaviors. The constitutive equations governing the system are derived and explained. We show how such a physical system turns out to be governed by a subtle interplay between four characteristic time scales.

We investigated the influence of the size of the NP: For small NPs (diameter <30 nm), the temperature rise is not as high as expected due to fast heat release. For bigger NPs, the temperature rise is damped because large NPs are not efficient absorbers. This leads to a particle size compromise of $\sim$40 nm that optimizes the temperature increase (for a given laser irradiance).

The role of a possible molecular coating is also investigated in detail based on considerations on interface thermal resistivity. For high interface resistivity, a temperature damping is observed outside the NP while an enhanced temperature increase is observed inside. A high interface resistivity tends in parallel to slow down the heat release in the surrounding medium, making the heating of the surroundings less efficient.

A detailed comparison between cw and pulsed illumination was drawn and two main results were obtain: (i) While a temperature profile in $1/r$ in the surrounding medium is observed under cw illumination, a much more confined temperature envelope in $1/r^3$ characterizes a pulsed illumination. A refined model even further demonstrates a higher degree of confinement with a spatial profile following a stretched exponential. (ii) Unexpectedly, pulsed illumination does not necessarily achieve much higher-temperature increase in the surroundings compared to cw, especially for nanoparticles larger than 100 nm (typically lithographic plasmonic structures). It can even be worse when the gold particle is endowed with a poor thermal surface conductivity (due to an hydrophobic molecular coating, for example).

Finally, the influence of the repetition rate is discussed and two regimes are identified depending on the NP radius R and the pulse repetition rate f: one time-localization regime, where the temperature increase is confined spatially and temporally, and one regime that tends to resemble to the regime observed under cw illumination.

Within this work, we restricted ourselves to gold NPs with spherical geometry (radius R), but most of the results obtained herein are also valid for nonspherical particles when considered as particles of characteristic size R. The numerical techniques we developed could also be refined to address problems with 2D symmetries requiring a longer computation time. This versatile numerical technique could also take into

account other materials than gold and water and various pulse durations, from femtosecond to nanosecond scales.

ACKNOWLEDGMENT

We thank Jon Donner, Christian Girard, Julien Polleux, Philippe Réfrégier, Damien Riedel, and Jérôme Wenger for helpful discussions.

APPENDIX: NUMERICAL ALGORITHM

In this Appendix, we explain and detail how the physical system was modeled using a FDM and in particular what the RK4 algorithm consists in.

We shall specifically use in this Appendix the equations and the formalism based on dimensionless space and time variables (ρ and τ) and dimensionless constants and parameters (β, γ, and λ_K).

1. Model assuming a uniform NP temperature

We consider in this part a spherical NP endowed with a surface conductivity g and characterized by a uniform inner temperature $T_{NP}(\tau)$. This problem is described by the set of Eqs. (36). Since the NP temperature is assumed to be uniform, only the surrounding medium has to be meshed (see Fig. 9). The spatiotemporal meshing of the system is such that

$$\rho_i \equiv 1 + i \times \delta\rho, \quad i \in [0,N],$$
$$\tau_j \equiv j \times \delta\tau, \quad j \in [0,M],$$
$$T_{i,j} \equiv T(\rho_i,\tau_j).$$

To simplify the notations and the explanations, we consider here a regular spatiotemperal mesh. However, it would be wise to use, for instance, a refined mesh close the NP interface and a rougher mesh further.

The boundary condition (36) at the NP interface reads

$$-\frac{T_{2,j} - T_{1,j}}{\delta\rho} = \frac{T_{0,j} - T_{1,j}}{\lambda_K}. \tag{A1}$$

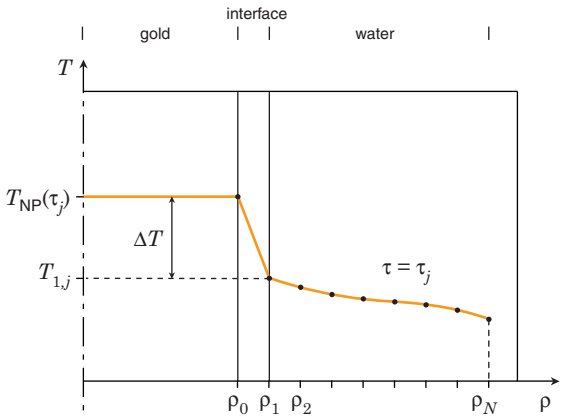

FIG. 9. (Color online) Schematic of the temperature profile at time τ_j around a spherical gold NP as modeled in the FDM-RK4 algorithm. In this first model, the NP temperature $T_{NP}(\tau_j)$ is assumed to be uniform and a temperature discontinuity ΔT occurs at the nanoparticle interface to take into account a finite interface conductivity.

The temperature drop ΔT occurs between the coordinates ρ_0 and ρ_1. The temperature gradient on the NP surface is calculated between the coordinates ρ_1 and ρ_2 (see Fig. 9).

The initial temperature profile is set to

$$T_{0,0} = T^0_{NP}, \tag{A2}$$

$$T_{1,0} = \frac{T^0_{NP}}{1 + \delta\rho/\lambda_K}, \tag{A3}$$

$$T_{i,0} = 0 \quad \text{for } i > 1. \tag{A4}$$

This initial temperature profile corresponds to a zero temperature outside the NP and fulfills the boundary condition (A1).

The numerical algorithm consists of a spatial loop over the position i inside a temporal loop over the time j. At each time $j+1$, the procedure is as follows.

First, the NP temperature $T_{0,j+1}$ is calculated from the second equation of system (36):

$$T_{0,j+1} = T_{0,j} + 3\beta\,\delta\tau\,\frac{T_{2,j} - T_{1,j}}{\delta\rho}. \tag{A5}$$

Then, using Eq. (A1), one can compute the temperature on the NP surface ($i = 1$):

$$T_{1,j+1} = \frac{l_K T_{2,j} + \delta\rho T_{0,j+1}}{\lambda_K + \delta\rho}. \tag{A6}$$

Finally, the computation of the temperature profile in the surrounding medium ($i > 2$) is performed according to the RK4 procedure[43]

$$T_{i,j+1} = T_{i,j} + \frac{k_1 + 2k_2 + 2k_3 + k_4}{6}, \tag{A7}$$

where

$$k_1 = \delta t\ K(T_{i,j}),$$
$$k_2 = \delta t\ K(T_{i,j} + k_1/2),$$
$$k_3 = \delta t\ K(T_{i,j} + k_2/2),$$
$$k_4 = \delta t\ K(T_{i,j} + k_3),$$

and

$$K(T_{i,j}) = \frac{2}{\rho}\frac{T_{i+1,j} - T_{i,j}}{\delta\rho} + \frac{T_{i+1,j} - 2T_{i,j} + T_{i-1,j}}{\delta\rho^2}. \tag{A8}$$

Note that the increments $\delta\rho$ and $\delta\tau$ cannot be chosen arbitrarily and independently. To ensure a proper convergence, $\delta\rho$ and $\delta\tau$ have to be chosen much smaller than unity while fulfilling as well the convergence criteria:

$$\delta\rho^2/\delta\tau \gg 1. \tag{A9}$$

This ensures that the right-hand member of equation (A7)—the variation of the NP temperature—is small compared to the NP temperature $T_{i,j}$.

It is worth estimating the total energy of the system and its conservation at each time step to check the consistency of the calculations. The normalized energy at time τ_j expressed from Eq. (40) reads

$$\epsilon_j = \frac{T_{0,j}}{T_{0,0}} + 3\beta\delta\rho\sum_{i=1}^{N}\rho_i^2\frac{T_{i,j}}{T_{0,0}} \tag{A10}$$

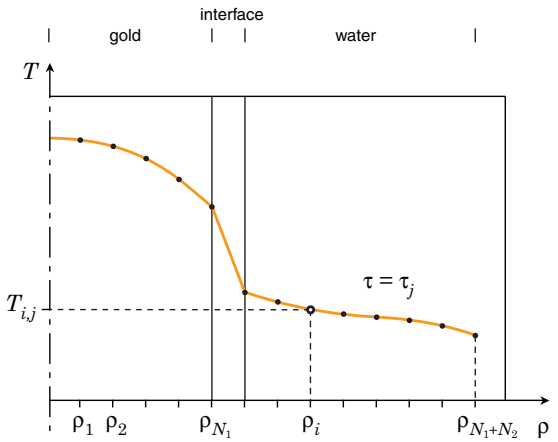

FIG. 10. (Color online) Schematic of the temperature profile at time τ_j around a spherical gold NP as modeled in the FDM-RK4 algorithm. In this second model, the temperature inside the NP is also meshed.

and should remain close to unity at any step j of the numerical procedure.

2. Model including a nonuniform NP temperature and a zero initial temperature profile

We assume in this section that the inner temperature of the NP is not necessarily uniform. We shall also explain how both the heating and cooling of the NP can be investigated numerically.

In this context, the normalized coordinate now reads

$$\rho_i \equiv i \times \delta\rho, \quad i \in [0, N_1 + N_2 - 1],$$

and in particular $\rho_{N_1} = N_1 \times \delta\rho = 1$. N_1 is the number of mesh points in the NP and N_2 in the surrounding medium (see Fig. 10).

To simplify the notations and the explanations, we consider here a regular mesh. However, it would make sense to use, for instance, a rough mesh inside the NP and a refined mesh in the surrounding medium, close to the NP interface.

The discretized boundary conditions of system (12) yield this time

$$\frac{T_{N_1+2,j} - T_{N_1+1,j}}{\delta\rho} = -\frac{T_{N_1,j} - T_{N_1+1,j}}{\lambda_K} = \gamma \frac{T_{N_1,j} - T_{N_1-1,j}}{\delta\rho}. \tag{A11}$$

At time τ_0, the initial temperature profile is set to zero:

$$\forall i, \quad T_{i,0} = 0.$$

At time τ_{j+1}, the calculation of the temperature profile inside the NP ($i < N_1$) is performed using the RK procedure [Eq. (A7)] and replacing the RK function $K(T_{i,j})$ with

$$K_{\mathrm{Au}}(T_{i,j}) = \beta\gamma K(T_{i,j}) + p_0(\tau_j).$$

This source term $p_0(\tau_j)$ has to be added when one wants to take into account a heat generation in the NP. For a pulsed illumination, it reads

$$p_0(\tau_j) = T^0_{\mathrm{NP}} \frac{\tau_{\mathrm{p}}}{\tau_{\text{e-ph}}} \exp(-\tau_j \tau_{\mathrm{p}}/\tau_{\text{e-ph}}).$$

And for a cw illumination

$$p_0 = 3\beta T^{\mathrm{cw}}_{\mathrm{NP}}.$$

The convergence criteria is now

$$\delta\rho^2/\delta\tau \gg \beta\gamma \approx 860. \tag{A12}$$

This means that while investigating the dynamics of the NP temperature, the convergence criteria is more drastic. However, this is expected and not an issue since the associated time scale of the temperature diffusion inside the NP is much faster. Consequently, $\delta\tau$ can be chosen much smaller.

Then the temperatures at the nanoparticle interface $T_{N_1,j}$ and $T_{N_1+1,j}$ have to be calculated using the boundary conditions (A11). This yields

$$T_{N_1,j+1} = \frac{\gamma(\delta\rho + \lambda_K)T_{N_1-1,j} + \delta\rho T_{N_1+2,j}}{\gamma\lambda_K + \delta\rho + \gamma\delta\rho},$$

$$T_{N_1+1,j+1} = T_{N_1+2,j} + \gamma(T_{N_1-1,j} - T_{N_1,j+1}).$$

Finally the temperature profile within the surrounding medium ($i > N_1 + 1$) is computed using the RK4 procedure [Eq. (A7)] and the regular RK function $K(T_{i,j})$ [Eq. (A8)].

When considering an initial zero temperature profile, the energy conservation laws (43) and (44) now reads for cw illumination

$$3\beta T^{\mathrm{wc}}_{\mathrm{NP}} j\delta\tau = \sum_{i=0}^{N_1} 3\rho_i^2 T_{i,j}\delta\rho + \sum_{i=N_1+1}^{N_1+N_2} 3\beta\rho_i^2 T_{i,j}\delta\rho.$$

And with pulsed illumination

$$T^0_{\mathrm{NP}}\left[1 - \exp\left(\frac{-\tau_j \tau^{\mathrm{w}}_{\mathrm{d}}}{\tau_{\mathrm{e-ph}}}\right)\right] = \sum_{i=0}^{N_1} 3\rho_i^2 T_{i,j}\delta\rho + \sum_{i=N_1+1}^{N_1+N_2} 3\beta\rho_i^2 T_{i,j}\delta\rho.$$

*guillaume.baffou@fresnel.fr

[1] A. O. Govorov and H. H. Richardson, Nano Today **2**, 30 (2007).
[2] G. Baffou, R. Quidant, and F. J. García de Abajo, ACS Nano **4**, 709 (2010).
[3] A. Nitzan and L. E. Brus, J. Chem. Phys. **75**, 2205 (1981).
[4] W. A. Challener, C. Peng, A. V. Itagi, D. Karns, W. Peng, Y. Peng, X. M. Yang, X. Zhu, N. J. Gokemeijer, Y.-T. Hsia, G. Ju, R. E. Rottmayer, M. A. Seigler, and E. C. Gage, Nat. Photon. **3**, 220 (2009).
[5] L. Cao, D. Barsic, A. Guichard, and M. Brongersma, Nano Lett. **7**, 3523 (2007).
[6] D. Pissuwan, S. M. Valenzuela, and M. B. Cortie, Trends Biotechnol. **24**, 62 (2006).
[7] P. K. Jain, I. H. El-Sayed, and M. A. El-Sayed, Nano Today **2**, 18 (2007).

[8]S. Lal, S. E. Clare, and N. J. Halas, Acc. Chem. Res. **41**, 1842 (2009).
[9]G. Han, P. Ghosh, M. De, and V. M. Rotello, NanoBioTechnology **3**, 40 (2007).
[10]A. G. Skirtach, C. Dejugnat, D. Braun, A. S. Susha, A. L. Rogach, W. J. Parak, H. Möhwald, and G. B. Sukhorukov, Nano Lett. **5**, 1371 (2005).
[11]L. Tong, Q. Wei, A. Wei, and J. X. Cheng, Photochem. Photobiol. **85**, 21 (2009).
[12]J. Butet, J. Duboisset, G. Bachelier, I. Russier-Antoine, E. Benichou, C. Jonin, and P. F. Brevet, Nano Lett. **10**, 1717 (2010).
[13]W. Lu, Q. Huang, G. Ku, X. Wen, M. Zhou, D. Guzatov, P. Brecht, R. Su, A. Oraevsky, L. V. Wang, and C. Li, Biomaterials **31**, 2617 (2010).
[14]S. Mallidi, T. Larson, J. Aaron, K. Sokolov, and S. Emelianov, Opt. Express **15**, 6583 (2007).
[15]A. Vogel and V. Venugopalan, Chem. Rev. **103**, 577 (2003).
[16]R. R. Anderson and J. A. Parrish, Science **220**, 524 (1983).
[17]V. K. Pustovalov, Chem. Phys. **308**, 103 (2005).
[18]A. N. Volkov, C. Sevilla, and L. V. Zhigilei, Appl. Surf. Sci. **253**, 6394 (2007).
[19]M. Hu and G. V. Hartland, J. Phys. Chem. B **106**, 7029 (2002).
[20]M. Hu, X. Wang, G. V. Hartland, P. Mulvaney, J. P. Juste, and J. E. Sader, J. Am. Chem. Soc. **125**, 14925 (2003).
[21]A. L. Tchebotareva, P. V. Ruijgrok, and M. Orrit, Laser Photon. Rev. **4**, 581 (2010).
[22]N. Large, L. Saviot, J. Margueritat, J. Gonzalo, C. N. Afonso, A. Arbouet, P. Langot, A. Mlayah, and J. Aizpurua, Nano Lett. **9**, 3732 (2009).
[23]P. Chakravarty, W. Qian, M. A. El-Sayed, and M. R. Prausnitz, Nat. Nanotech. **5**, 607 (2010).
[24]A. Vogel, J. Noack, G. Hüttman, and G. Paltauf, Appl. Phys. B **81**, 1015 (2005).
[25]D. Lapotko, Opt. Express **17**, 2538 (2009).
[26]E. Lukianova-Hleb, L. Hu, Y. Latterini, L. Tarpani, S. Lee, R. A. Drezek, J. H. Hafner, and D. O. Lapotko, ACS Nano **4**, 2109 (2010).
[27]A. Vogel, N. Linz, S. Freidank, and G. Paltauf, Phys. Rev. Lett. **100**, 038102 (2008).
[28]V. Kotaidis, C. Dahmen, G. von Plessen, F. Springer, and A. Plech, J. Chem. Phys. **124**, 184702 (2006).
[29]S. Link, C. Burda, B. Nikoobakht, and M. A. El-Sayed, J. Phys. Chem. B **104**, 6152 (2000).
[30]E. Lukianova-Hleb, L. J. E. Anderson, S. Lee, J. H. Hafner, and D. O. Lapotko, Phys. Chem. Chem. Phys. **12**, 12237 (2010).
[31]A. Plech, V. Kotaidis, S. Grésillon, C. Dahmen, and G. von Plessen, Phys. Rev. B **70**, 195423 (2004).
[32]E. Sassaroli, K. C. P. Li, and B. E. O'Neill, Phys. Med. Biol. **54**, 5541 (2009).
[33]E. Y. Hleb and D. O. Lapotko, Nanotechology **19**, 355702 (2008).
[34]O. Ekici, R. K. Harrison, N. J. Durr, D. S. Eversole, M. Lee, and A. Ben-Yakar, J. Phys. D **41**, 185501 (2008).
[35]M. Hu, H. Petrova, and G. V. Hartland, Chem. Phys. Lett. **391**, 220 (2004).
[36]S. Merabia, P. Keblinski, L. Joly, L. J. Lewis, and J. L. Barrat, Phys. Rev. E **79**, 021404 (2009).
[37]S. Merabia, S. Shenogin, L. Joly, P. Keblinski, and J. L. Barrat, Proc. Natl. Acad. Sci. USA **106**, 15113 (2009).
[38]A. J. Schmidt, J. D. Alper, M. Chiesa, G. Chen, S. K. Das, and K. Hamad-Schifferli, J. Phys. Chem. C **112**, 13320 (2008).
[39]O. M. Wilson, X. Hu, D. G. Cahill, and P. V. Braun, Phys. Rev. B **66**, 224301 (2002).
[40]Z. Ge, D. G. Cahill, and P. V. Braun, J. Phys. Chem. B **108**, 18870 (2010).
[41]J. Alper and K. Hamad-Schifferli, Langmuir **26**, 3786 (2010).
[42]W. Benenson, J. W. Harris, H. Stocker, and H. Lutz (eds.), *Handbook of Physics* (Springer-Verlag, New York, 2000).
[43]J. C. Butcher, *Numerical Methods for Ordinary Differential Equations* (Wiley, Hoboken, NJ, 2003).
[44]G. Baffou, R. Quidant, and C. Girard, Phys. Rev. B **82**, 165424 (2010).
[45]P. K. Jain, K. S. Lee, I. H. El-Sayed, and M. A. El-Sayed, J. Phys. Chem. B **110**, 7238 (2006).
[46]C. F. Bohren and D. R. Huffman, *Absorption and Scattering of Light by Small Particles* (Wiley Interscience, New York, 1983).
[47]V. Myroshnychenko, J. Rodríguez-Fernández, I. Pastoriza-Santos, A. M. Funston, C. Novo, P. Mulvaney, L. M. Liz-Marzán, and F. J. García de Abajo, Chem. Soc. Rev. **37**, 1792 (2008).
[48]P. Grua, J. P. Morreeuw, H. Bercegol, G. Jonusauskas, and F. Vallée, Phys. Rev. B **68**, 035424 (2003).
[49]H. Inouye, K. Tanaka, I. Tanahashi, and K. Hirao, Phys. Rev. B **57**, 11334 (1998).
[50]A. Arbouet, C. Voisin, D. Christofilos, P. Langot, N. Del Fatti, F. Vallée, J. Lermé, G. Celep, E. Cottancin, M. Gaudry, M. Pellarin, M. Broyer, M. Maillard, M. P. Pileni, and M. Treguer, Phys. Rev. Lett. **90**, 177401 (2003).
[51]W. Huang, W. Qian, M. A. El-Sayed, Y. Ding, and Z. L. Wang, J. Phys. Chem. C **111**, 10751 (2007).
[52]J. H. Hodak, A. Henglein, and G. V. Hartland, J. Chem. Phys. **111**, 8613 (1999).
[53]S. Link, C. Burda, Z. L. Wang, and M. A. El-Sayed, J. Chem. Phys. **111**, 1255 (1999).
[54]Z. Ge, D. G. Cahill, and P. V. Braun, Phys. Rev. Lett. **96**, 186101 (2006).
[55]G. Baffou, R. Quidant, and C. Girard, Appl. Phys. Lett. **94**, 153109 (2009).